Competing High-Temperature Deformation Mechanisms in Mo(Si,Al)<inf>2</inf>–Al<inf>2</inf>O<inf>3</inf> Composites

Competing High-Temperature Deformation Mechanisms in $Mo(Si,Al)_2$–Al_2O_3 Composites

AINA EDGREN, ERIK STRÖM, and MAGNUS HÖRNQVIST COLLIANDER

$Mo(Si,Al)_2$–Al_2O_3 composites were tested in four-point bending at 1300 °C. The addition of Al_2O_3 led to a decrease in grain size, and a subsequent decrease in strength for materials containing up to 15 wt pct Al_2O_3. At higher Al_2O_3 fractions, the decrease in grain size saturates and the strength is recovered as the Al_2O_3 particles prevent grain boundary sliding.

https://doi.org/10.1007/s11661-024-07520-7

$Mo(Si,Al)_2$ is a ceramic material with high resistivity, high melting point and excellent oxidation properties in both oxidizing and reducing environments.[1–4] The main application is as heating elements in electrical furnaces. Therefore, the material is often considered to be a cornerstone in the ongoing process of reducing the emission of greenhouse gasses, facilitating the transition from fossil-gas-driven furnaces to electrical alternatives. However, an inherent challenge lies in the mechanical properties of $Mo(Si,Al)_2$.

$Mo(Si,Al)_2$ has a high ductile to brittle transition temperature (DBTT), 1250 °C for polycrystalline C40, above which the yield stress decreases rapidly with an increase in temperature.[5,6] The low yield stress becomes problematic when scaling up the size of heating elements for industrial furnaces operating in the MW range, as the gravitational force on the elements increases, potentially leading to excessive deformation.

In order to make $Mo(Si,Al)_2$ suitable for use as large heating elements, the mechanical properties need to be both understood and improved. A promising way to improve the high-temperature strength is the addition of a secondary phase, as this could provide a particle-strengthening effect. This strategy has proven successful in $MoSi_2$, a material similar to $Mo(Si,Al)_2$.[7–13] We have previously investigated the effects of particle additions on the mechanical properties of $Mo(Si,Al)_2$ through compression testing of $Mo(Si,Al)_2$–Al_2O_3 composites (containing 0 to 25 wt pct Al_2O_3) at 1300 °C[14,15] using a Gleeble thermomechanical simulator.

The addition of Al_2O_3 led to a decrease in strength for additions up to 15 wt pct, whereas higher Al_2O_3 contents (20 and 25 wt pct) led to a recovery of the strength. The addition of Al_2O_3 particles reduced the grain size, and the fine-grained $Mo(Si,Al)_2$–Al_2O_3 composites did not show the same extent of intergranular misorientation as the coarse-grained Al_2O_3-free material in the deformed state. It was therefore suggested that the decreasing grain size caused a transition in the deformation mechanism from dislocation slip to diffusion-based creep. This could partly explain the initial reduction in strength when 5 wt pct Al_2O_3 was added, but for higher additions, the measured grain size remained constant, while the strength continued to decrease until the minimum at 15 wt pct.

This suggests that there are other mechanisms at play, and it was hypothesized that electroplasticity, caused by the resistive heating used in the Gleeble, played a role. In both ceramics and metals, it has been shown that electroplasticity locally heats and creates charge imbalance over grain boundaries, thereby locally weakening bonds[16–19] and promoting grain boundary sliding. Given that the effective conductive area in a cross-section decreases with the addition of Al_2O_3 with negligible electric conductivity, electroplasticity effects were proposed to become more pronounced with increasing additions. Simultaneously, however, the increased addition of particles, which primarily reside on grain boundaries due to the processing route, will lead to particle strengthening through pinning of the boundaries. At higher Al_2O_3 contents (20 and 25 wt pct), the strengthening effect of the Al_2O_3 particles outweighed the proposed electroplasticity-induced softening, resulting in improved performance compared to Al_2O_3 lean materials.

Electroplasticity-induced softening could be detrimental to the use of $Mo(Si,Al)_2$ as resistive heating elements.

AINA EDGREN is with the Department of Physics, Chalmers University of Technology, 41296 Gothenburg, Sweden and also with the Kanthal AB, 73427 Hallstahammar, Sweden. Contact e-mail: aina.edgren@chalmers.se ERIK STRÖM is with the Kanthal AB, 73427 Hallstahammar, Sweden. MAGNUS HÖRNQVIST COLLIANDER is with the Department of Physics, Chalmers University of Technology, 41296 Gothenburg, Sweden.
Manuscript submitted January 10, 2024; accepted July 7, 2024.
Article published online July 23, 2024

Table I. Average Density of the Sintered Materials

Material	Wt Pct Mo $(Si,Al)_2$	Wt Pct Al_2O_3	Density (g cm^{-3})	Pct of Theoretical Density
A5	95	5	5.75	98.1
A15	85	15	5.49	98.2
A25	75	25	5.21	97.7
A30	70	30	5.10	97.5

In order to test the electroplasticity hypothesis, mechanical testing of $Mo(Si,Al)_2$–Al_2O_3 composites with varying particle content must be performed without electric heating. Here we perform four-point bending tests of composites containing 5 to 30 wt pct Al_2O_3 at 1300 °C. The specimens were heated by external radiative heating instead of resistive heating to avoid electroplasticity. The composites were prepared from the same $Mo(Si,Al)_2$ and Al_2O_3 powders as the composites investigated in References 15 and 14, and synthesized in an identical way.

$Mo(Si,Al)_2$ was synthesized by dry mixing of elemental Mo (99.9 pct purity, Cerac Inc.), Si (99.99 pct purity, Wacker) and Al (99.5 pct purity, GoodFellow) powders in a Mo-lined ball mill with Mo balls. The powder mixture was heated in inert Ar gas to initiate a self-propagating reaction in which $Mo(Si,Al)_2$, as well as small amounts of $Mo_5(Si,Al)_3$ and Al_2O_3 (approximately 1.7 vol pct[14]), were formed. The reaction product underwent milling in an Mo metal ball mill for 228 hours to achieve a fine-grained powder with an average particle size of approximately 5 μm.

Four $Mo(Si,Al)_2$–Al_2O_3 composites, containing 5, 15, 25 and 30 wt pct Al_2O_3 respectively, were prepared by adding Al_2O_3 particles (AKP-53, Sumitomo Chemical, purity: 99.99 pct) to the milled $Mo(Si,Al)_2$ powder. To prevent agglomeration of the Al_2O_3 particles, the powders were milled for 1 minutes in a vibratory steel disc mill. The powders were compacted to rods using a cold isostatic press (CIP, EPSI) operating at 2000 bar, prior to sintering for 1 hour at 1650 °C in H_2 gas in a tube furnace. The as-sintered materials had densities (measured using Archimedes' method) of around 98 pct of the theoretical values, see Table I.

The rods were cut and ground to bars ($3 \times 4 \times 50$ mm^3). For each composite, at least five bars were subjected to high-temperature four-point bending tests at Fraunhofer IKTS in Dresden, Germany, in a vacuum of 10^{-5} mbar at 1300 °C, using a Shimadzu AG-20kNG testing machine. The tests were carried out according to the DIN EN 820-1 standard. The cross-head speed was 0.5 mm min^{-1} (initial strain rate was 1.25×10^{-4} s^{-1}), the loading span 20 mm and the support span 40 mm. The deflection was measured at the loading points. The maximum deflection was around 1 mm due to the geometric constraints of the test rig.

For materials characterization, an FEI Quanta 200 FEG ESEM scanning electron microscope (SEM) operating at 20 kV was used for microstructure imaging and chemical composition analysis using energy-dispersive X-ray spectroscopy (EDS). Electron backscatter diffraction (EBSD) was used for additional microstructural investigation in a Tescan GAIA 3 SEM operating at an acceleration voltage of 15 kV.

The chemical composition of $Mo(Si,Al)_2$ was 32 at. pct Mo, 37 at. pct Si, 29 at. pct Al, as well as small amounts of O, C and Fe (< 0.03 at. pct). Phase maps acquired using EBSD are shown in Figure 1. The phase volume fractions of the composites are shown in Table II. Two $Mo_5(Si,Al)_3$ phases, with $D8_m$ and $D8_8$ structure, were present in small amounts. $D8_m$ is commonly reported in $Mo(Si,Al)_2$ materials and is a result of local chemical variations in the unreacted powder,[4,20,21] whereas $D8_8$ is stabilized by C[22–24] and presumably a result of contaminations during synthesis. Although the volume fractions of the minority phases differed slightly between materials, the low volume fractions are not expected to significantly affect the mechanical properties of the composites.

The grain size histograms in $Mo(Si,Al)_2$ in Figure 1 show that A15, A25 and A30 have relatively similar grain sizes, while the grains in A5 are slightly larger because of grain growth during sintering. The grain sizes in this study should also be compared with those reported in References 15 and 14 as the materials were synthesized identically. The 5 wt pct Al_2O_3 containing composite in Reference 15 was reported to have a grain size of 7.1 μm, which is significantly smaller than that reported for 5 wt pct addition here. Additional EBSD investigations were therefore performed on the 5 wt pct sample. The average grain sizes from individual EBSD maps varied significantly, with values as high as 10.0 μm. This indicates that an addition of 5 wt pct is not enough to obtain a homogeneous microstructure. The higher Al_2O_3-containing composites had a smaller and more even grain size, as grain boundary pinning by the oxide particles limits grain growth during sintering, although the distribution was somewhat broader in the material with 15 wt pct Al_2O_3 compared to 25 and 30 wt pct, see Figure 1 and Reference 15.

All composites exhibited plastic deformation during four-point bending testing. A photo of a tested A5 specimen is shown in Figure 2(a). Optical microscopy (OM) did not show any cracks on the surface. The flexural stress, σ_f, was calculated using Eq. [1][25]

$$\sigma_f = \frac{3}{4}\frac{FL}{bd^2} \quad [1]$$

where F is the force, b is the sample width and d is the thickness of the bending bar. The equation is valid for bending bars having a load span of 1/2 of the support

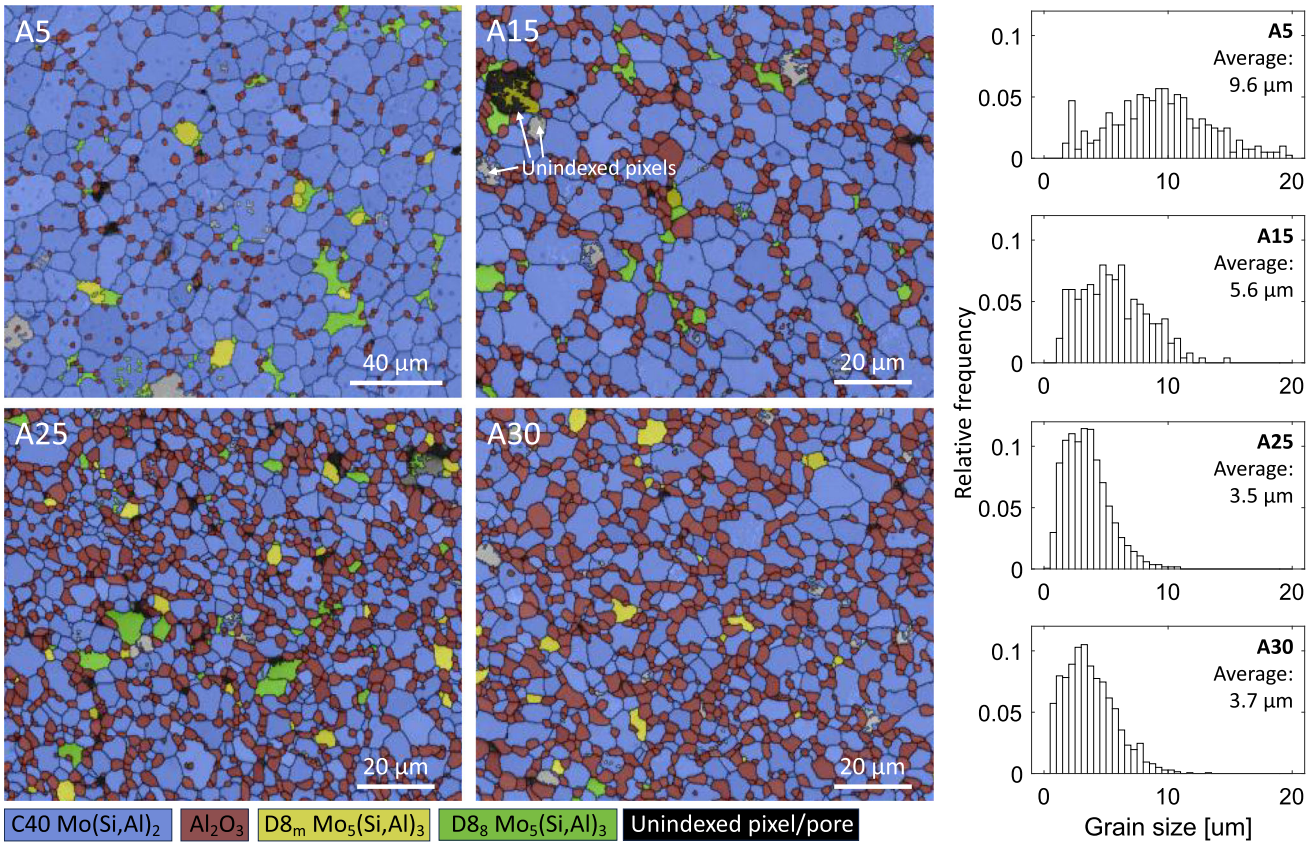

Fig. 1—EBSD phase maps and grain size histograms of A5, A15, A25, A30. Note the different magnification for the map of A5 compared to the other materials.

Table II. Phase Volume Fraction and Grain Size, Acquired Using EBSD, of Sintered Composites

Material	Phase Volume Fraction [Pct]					Grain Size C40 [μm] (Standard Deviation)
	C40 $Mo(Si,Al)_2$	α-Al_2O_3	$D8_m$ $Mo_5(Si,Al)_3$	$D8_8$ $Mo_5(Si,Al)_3$	Pores or Not Indexed	
A5	84	7.1	0.7	6.0	2.2	9.6 (4.38)
A15	69	23	0.2	5.9	1.9	5.6 (2.66)
A25	62	32	2.0	2.3	2.0	3.5 (1.52)
A30	57	38	2.4	0.2	1.9	3.7 (2.02)

span (L) and positioned symmetrically between the supports. The resulting stress-displacement curves are shown in Figure 2(b). Small marks from the load and support rolls were visible on the tested specimens, see Figure 2(a). In the case of A5, only four curves are shown, the fifth was rejected because of misalignment of the specimen in the sample holder. It was noted that the load span was shifted by 1 mm towards one of the support rolls. This could be due to the mobility of the rollers and the rotatability of the upper punch, which are demands from the standard, in combination with thermal expansion. However, the same shift was observed for all specimens. Hence, the values in Figure 2(a) are not absolute, but still give a good estimation of the flexural stress. The data in Figure 2(a) has also been filtered using a band stop filter as the raw data was slightly affected by temperature fluctuations in the furnace. The raw data as well as further details on the data processing are found in the electronic supplementary material. The abrupt stress drops are the result of the setting of the rollers due to the thermal expansion. We note that after a stress drop, there is a "recovery" period before the stress returns to the response expected from the extrapolation of the curve before the drop.

Figure 2(b) shows that the stress levels decrease as the Al_2O_3 content increases from 5 to 15 wt pct. Conversely, as Al_2O_3 content increases from 15 to 25 and 30 wt pct, the stress increases. Figure 3 shows the flexural stress at two different deformation levels, corresponding to a permanent displacement of the loading rolls of 0.04 and 0.4 mm (equal to 0.2 and 2 pct of the loading span distance, respectively), as well as the maximum stress for

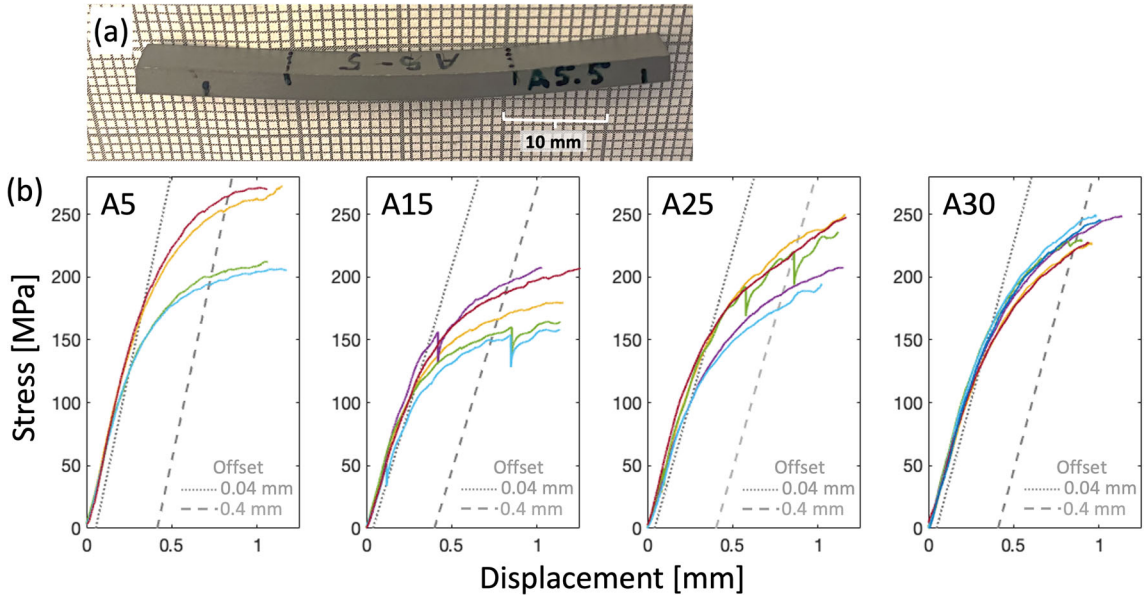

Fig. 2—(*a*) Photo of A5 specimen after deformation. The position of load and support rolls are indicated, (*b*) stress–displacement curves of the $Mo(Si,Al)_2$–Al_2O_3 composites with lines corresponding to offsets of 0.04 and 0.4 mm, respectively.

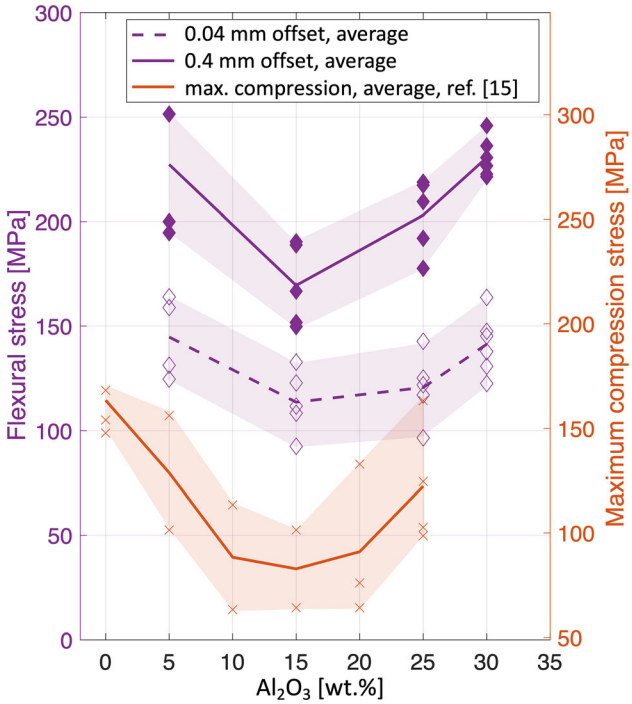

Fig. 3—Diamond marks: flexural stress values corresponding to a permanent deformation equal to a displacement of 0.04 mm (not filled) and 0.4 mm (filled) of the load span distance. Cross marks: maximum compression stress from Ref. [15]. The lines show the average stress values for the tested specimens.

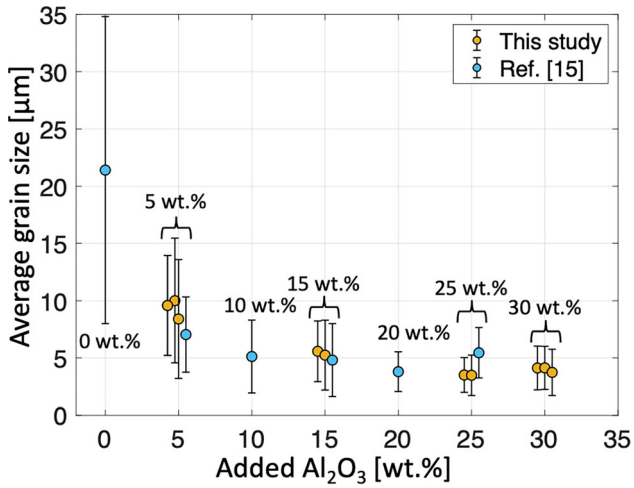

Fig. 4—Average $Mo(Si,Al)_2$ grain size with error bars as a function of Al_2O_3 content from this study and Ref. [15]. The data points have been shifted vertically for improved readability.

the resistively heated samples from Reference 15. The same behavior, a gradual decrease in strength for composites containing up to 15 wt pct Al_2O_3, followed by an increase at higher Al_2O_3 contents, is observed in both cases. As external heating, where electroplasticity cannot occur, was used in the present study, we conclude that the deformation behavior is not controlled by electroplasticity. Instead, the decreasing strength with increasing particle fraction can be explained by the decreasing grain size (from 9.6 in A5 to 5.6 μm in A15). Figure 4 shows the grain size as a function of wt pct Al_2O_3 from both the current study and [15], where the average grain size obtained from different EBSD maps is shown as separate data points. The grain size saturates around 10 to 15 wt pct, but due to the limited number of observed regions in Reference 15 we previously concluded that the saturation occurred already at around 5 wt pct, leading to the suggestion of the additional mechanism of electroplasticity. Above 15 wt pct, the grain size saturates and the particle strengthening effect dominates, where the Al_2O_3 particles in grain

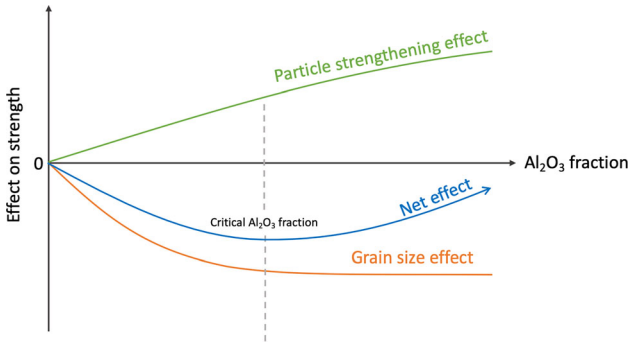

Fig. 5—Schematic illustration of the effect of grain size and Al_2O_3 particle strengthening on the strength.

boundaries inhibit sliding. Grain boundary sliding has been shown to be the dominating deformation mechanism in fine-grained $MoSi_2$,[10,13] and is suggested to play an important role also in the deformation of $Mo(Si,Al)_2$, as only one slip system is active at high temperature.[26] The effect of grain size and particle strengthening on the strength as a function of added Al_2O_3 is schematically shown in Figure 5.

An important consequence of the observed behavior is that, if particle additions are used solely to prevent excessive grain growth and strength is not a primary concern in the design, a volume fraction of approximately 10 to 15 pct is required. We also note that the large variation in the grain size between different regions in the sample for low fractions of Al_2O_3 can introduce a dependence on the test method through the volume effect. In compression tests (*e.g.* Gleeble, used in our previous investigation[15]) the entire volume, comprising areas with both large and small grains, is subjected to a (nominally) uniform stress. During bending tests there is a stress gradient through the sample thickness, and only the outermost parts are subjected to the highest stress and will undergo plastic deformation. Consequently, while compression tests always measure the average response of regions with different grain size, the response of a bending test will depend on the grain size distribution in the limited volumes close to the outer surfaces. The presence or absence of volumes with large grains in the near-surface regions, which in the present case can be considered a statistical effect since the samples were machined from the interior of sintered rods, is expected to affect the measured strength. Hence, four-point bending might be more sensitive to an uneven grain size in the material. The volume effect is particularly important if test methods such as three-point bending are used, where there is also a gradient along the span length, and only a very small material volume experiences the maximum stress. Figure 2

While the stress trends (see Figure 3) are the same at low (0.04 mm offset) and high (0.4 mm offset) levels of deformation, the effect of Al_2O_3 increases with increasing plastic deformation. At 0.04 mm offset, only the decrease between 5 and 15 wt pct was statistically significant (two-sample t-test, significance level 5 pct). For higher Al_2O_3 contents, a significant difference in stress was observed only above an offset of 0.2 mm. This is reasonable as deformation primarily occurs by grain boundary sliding. To enhance understanding and model the behavior, it is important to identify the detailed deformation mechanism(s). This could be accomplished through additional experiments, such as testing the materials at different strain rates or in creep.

In summary, we have shown that:

- The dependence of the high temperature strength of $Mo(Si,Al)_2$–Al_2O_3 composites on the fraction of particle additions is a result of the competition between strength reduction due to grain refinement, and an increase due to grain boundary strengthening by particles. This leads to a strength minimum at intermediate fractions.
- Electroplasticity does not influence the mechanical properties of $Mo(Si,Al)_2$–Al_2O_3 composites, which is of importance for the use of the material as resistive heating elements.
- All Al_2O_3 additions lead to a decrease in grain size; however, 5 wt pct is insufficient to achieve a material with a homogeneous grain size. The grain size saturates at additions of around 10 to 15 wt pct.

FUNDING

Open access funding provided by Chalmers University of Technology. This research was funded by the Swedish Foundation for Strategic Research (SSF), Sweden and Kanthal AB, Sweden, through the industrial Ph.D. student Grant ID18-0064. The work was performed in part at Chalmers Materials Analysis Laboratory (CMAL).

OPEN ACCESS

CONFLICT OF INTEREST

The authors declare the following financial interests/personal relationships which may be considered as potential competing interests: Aina Edgren and Erik Ström are employees of Kanthal AB, a manufacturer of commercial heating elements.

SUPPLEMENTARY INFORMATION

The online version contains supplementary material available at https://doi.org/10.1007/s11661-024-07520-7.

REFERENCES

1. Sandvik Materials Technology: *Kanthal Super Electric Heating Elements*, Sandvik Materials Technology, Hallstahammar, 2012.
2. L. Ingemarsson, M. Halvarsson, J. Engkvist, T. Jonsson, K. Hellström, L.G. Johansson, and J.E. Svensson: *Intermetallics*, 2010, vol. 18, pp. 633–40.
3. M. Halvarsson, T. Jonsson, L. Ingemarsson, M. Sundberg, J.E. Svensson, and L.G. Johansson: *Mater. High Temp.*, 2009, vol. 26, pp. 137–43.
4. L. Ingemarsson, K. Hellström, S. Canovic, T. Jonsson, M. Halvarsson, L.G. Johansson, and J.E. Svensson: *J. Mater. Sci.*, 2013, vol. 48, pp. 1511–23.
5. K. Hagihara, T. Nakano, and Y. Umakoshi: *Scr. Mater.*, 1998, vol. 38, pp. 471–76.
6. Y. Umakoshi, T. Nakano, K. Kishimoto, D. Furuta, K. Hagihara, and M. Azuma: *Mater. Sci. Eng. A*, 1999, vol. 261, pp. 113–21.
7. Y. Suzuki, A. Nakahira, T. Sekino, and K. Niihara: *J. Jpn. Soc. Powder Powder Metall.*, 1996, vol. 43, pp. 272–77.
8. K. Niihara and Y. Suzuki: *Mater. Sci. Eng. A*, 1999, vol. 261, pp. 6–15.
9. R. Mitra, N.E. Prasad, S. Kumari, and A.V. Rao: *Metall. Mater. Trans. A*, 2003, vol. 34A, pp. 1069–88.
10. K. Sadananda, C.R. Feng, R. Mitra, and S.C. Deevi: *Mater. Sci. Eng. A*, 1999, vol. 261, pp. 223–38.
11. A. Newman, S. Sampath, and H. Herman: *Mater. Sci. Eng. A*, 1999, vol. 261, pp. 252–60.
12. K. Sadananda and C.R. Feng: *Mater. Sci. Eng. A*, 1995, vol. 192–193, pp. 862–67.
13. R. Mitra, K. Sadananda, and C.R. Feng: *Intermetallics*, 2004, vol. 12, pp. 827–36.
14. A. Edgren, E. Ström, R. Qiu, L. Frisk, F. Akhtar, and M. Hörnqvist Colliander: *Mater. Sci. Eng. A*, 2022, vol. 849, p. 143387.
15. A. Edgren, E. Ström, L. Frisk, F. Akhtar, and M. Hörnqvist Colliander: *Mater. Sci. Eng. A*, 2023, vol. 865, p. 144583.
16. O.A. Troitskii and V.I. Likhtman: *Dokl. Akad. Nauk SSR*, 1963, vol. 8, p. 91.
17. M.J. Kim, S. Yoon, S. Park, H.J. Jeong, J.W. Park, K. Kim, J. Jo, T. Heo, S.T. Hong, S.H. Cho, Y.K. Kwon, I.S. Choi, M. Kim, and H.N. Han: *Appl. Mater. Today*, 2020, vol. 21, p. 100874.
18. R. Fan, J. Magargee, P. Hu, and J. Cao: *Mater. Sci. Eng. A*, 2013, vol. 574, pp. 218–25.
19. J. Zhao: *Doctoral Thesis*, University of Akron, Akron, 2018.
20. M. Esmaeili Ghayoumabadi, A. Saidi, and M.H. Abbasi: *J. Alloys Compd.*, 2009, vol. 472, pp. 84–90.
21. T. Tabaru, K. Shobu, H. Hirai, and S. Hanada: *Intermetallics*, 2003, vol. 11, pp. 721–33.
22. A. Edgren, E. Ström, A. Rajagopal, and M. Hörnqvist Colliander: *Mater. Lett.*, 2023, vol. 353, p. 135219.
23. G. Zhang and X. Yue: *J. Mater. Sci.*, 2000, vol. 35, pp. 4729–33.
24. E. Parthe and W. Rieger: *J. Dent. Res.*, 1968, vol. 47, pp. 829–35.
25. W.D. Callister: *Materials Science and Engineering: An Introduction*, 7th ed. Wiley, New York, 2007.
26. H. Inui, M. Moriwaki, K. Ito, and M. Yamaguchi: *Philos. Mag. A*, 1998, vol. 77, pp. 375–94.